Journal of Medicinal Chemistry

pubs.acs.org/jmc

Article

Multitarget, Selective Compound Design Yields Potent Inhibitors of a Kinetoplastid Pteridine Reductase 1

Ina Pöhner,[§§] Antonio Quotadamo,[§§] Joanna Panecka-Hofman, Rosaria Luciani, Matteo Santucci, Pasquale Linciano, Giacomo Landi, Flavio Di Pisa, Lucia Dello Iacono, Cecilia Pozzi, Stefano Mangani, Sheraz Gul, Gesa Witt, Bernhard Ellinger, Maria Kuzikov, Nuno Santarem, Anabela Cordeiro-da-Silva, Maria P. Costi,* Alberto Venturelli,* and Rebecca C. Wade*

Cite This: *J. Med. Chem.* 2022, 65, 9011−9033

Read Online

ACCESS | Metrics & More | Article Recommendations | Supporting Information

ABSTRACT: The optimization of compounds with multiple targets is a difficult multidimensional problem in the drug discovery cycle. Here, we present a systematic, multidisciplinary approach to the development of selective antiparasitic compounds. Computational fragment-based design of novel pteridine derivatives along with iterations of crystallographic structure determination allowed for the derivation of a structure−activity relationship for multitarget inhibition. The approach yielded compounds showing apparent picomolar inhibition of *T. brucei* pteridine reductase 1 (PTR1), nanomolar inhibition of *L. major* PTR1, and selective submicromolar inhibition of parasite dihydrofolate reductase (DHFR) versus human DHFR. Moreover, by combining design for polypharmacology with a property-based on-parasite optimization, we found three compounds that exhibited micromolar EC_{50} values against *T. brucei brucei* while retaining their target inhibition. Our results provide a basis for the further development of pteridine-based compounds, and we expect our multitarget approach to be generally applicable to the design and optimization of anti-infective agents.

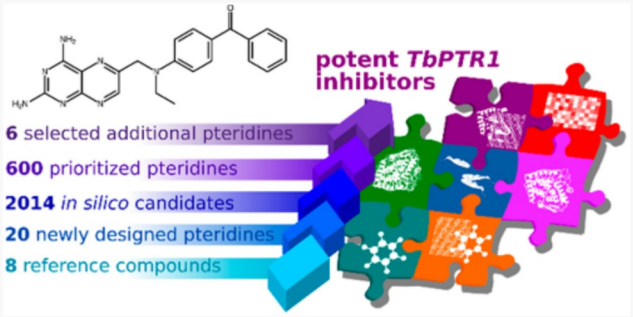

INTRODUCTION

The World Health Organization has identified 17 neglected tropical diseases (NTDs) that pose a health burden to over 1.4 billion people.[1,2] Parasites of the trypanosomatid family are responsible for two potentially lethal insect-vector borne NTDs: human African trypanosomiasis (HAT, sleeping sickness), caused by *Trypanosoma brucei*, and leishmaniasis, caused by the intracellular parasite *Leishmania spp.*[3−7] Current therapeutics are limited by toxicity, poor efficacy, and parasite resistance, thus underlining the need for new chemotherapies.[8,9]

New antiparasitic agents can be identified by target-based drug design strategies.[10−12] The folate pathway enzyme dihydrofolate reductase (DHFR) is a known anticancer, antibacterial, and antimalarial target.[13−16] It provides reduced folates, which are crucial to biological processes like DNA, protein, and amino acid synthesis or one-carbon transfer.[14,17,18] In trypanosomatids, DHFR inhibition, for example by methotrexate (MTX, **1a**), is ineffective due to a metabolic bypass via the biopterin-reducing pteridine reductase 1 (PTR1, Figure 1): when DHFR is inhibited, PTR1 is overexpressed and sustains sufficient reduced folate levels to ensure parasite survival. Thus, when targeting the folate pathway in *Leishmania*, both DHFR and PTR1 need to be considered.[19−21] In *T. brucei*, RNA interference studies have suggested PTR1 to be a potential antiparasitic target in its own right.[22,23] Nonetheless, even nanomolar PTR1 inhibitors have so far shown limited antiparasitic activity *in vitro*,[24,25] suggesting that targeting the *T. brucei* folate pathway may also benefit from the consideration of both PTR1 and DHFR.

Screening a set of folate-related compounds against parasitic folate pathway targets previously led to the identification of compounds **1b** (methyl-1-(4-(((2,4-diaminopteridin-6-yl)methyl)(methyl)amino)benzoyl)piperidine-4-carboxylate) and **1c** (methyl-1-(4-(((2,4-diaminopteridin-6-yl)methyl)amino)benzoyl)piperidine-4-carboxylate) as submicromolar inhibitors of *Leishmania major* PTR1 (*Lm*PTR1) with K_i values of 0.04 and 0.10 μM, respectively.[26] **1c** was additionally a micromolar inhibitor of *L. major* DHFR (*Lm*DHFR) with a weak selectivity for the parasite enzyme over the human DHFR (hDHFR) (K_i of 4 vs 10 μM). In contrast to the parasite DHFR, which is

Received: February 9, 2022
Published: June 8, 2022

https://doi.org/10.1021/acs.jmedchem.2c00232
J. Med. Chem. 2022, 65, 9011−9033

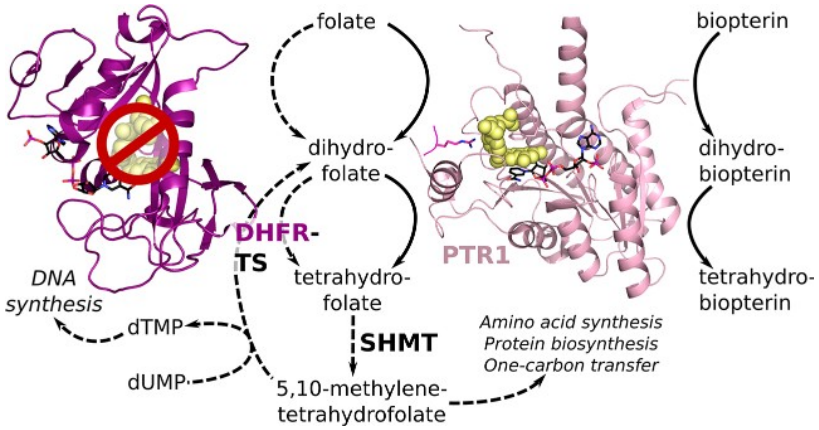

Figure 1. Overview of pterin activation in the trypanosomatidic folate pathway when DHFR is inhibited and PTR1 provides a metabolic bypass. Under normal conditions (indicated by dashed lines), the DHFR domain of the bifunctional DHFR-TS reduces biological folates to tetrahydrofolate (THF). Serine hydroxymethyl transferase (SHMT) converts THF to 5,10-methylene THF, which has a central role in amino acid synthesis, protein biosynthesis, and one-carbon transfer. It is also required by the TS domain of DHFR-TS to convert deoxyuridine monophosphate (dUMP) to deoxythymidine monophosphate (dTMP), which is necessary for DNA synthesis. PTR1 catalyzes the reduction of unconjugated pterins, like biopterin, and takes over folate reduction when DHFR is inhibited (continuous lines), thus acting as a metabolic bypass and an important additional target for shutting down the trypanosomatidic folate pathway. Both proteins are shown in cartoon representation (DHFR domain of DHFR-TS: purple, PTR1 monomer of the functional tetramer: light pink) with the NADPH/$NADP^+$ cofactor in a stick representation with black carbons and the folate substrate in yellow spheres. In PTR1, an arginine residue from a neighboring subunit that points into the active site is shown in a magenta stick representation.

covalently coupled with thymidylate synthase (TS) in a bifunctional DHFR-TS, the hDHFR off-target is monofunctional and shares only about 30% sequence identity with parasite DHFR domains, indicating potential for further optimization of selectivity.[27−29]

The current study focuses on optimizing pteridine-based compounds for their inhibition of *T. brucei* PTR1 (*Tb*PTR1) and *Tb*DHFR, in addition to the corresponding *Leishmania* targets, while ensuring selectivity against the off-target hDHFR. The enzymatic evaluation of reference pteridines reported earlier,[26,30] our comparative study of trypanosomatid folate pathway proteins,[31] and computational docking studies were first employed for the design of novel pteridine derivatives. Three new crystal structures of complexes of pteridines with *Tb*PTR1 and a complex with *Lm*PTR1 were determined and confirmed the predicted bound orientation of the novel pteridines. A systematic analysis of correlations between computed physicochemical molecular descriptors and observed antiparasitic effects was then performed and allowed us to prioritize promising compounds for synthesis. In total, we identified 26 new pteridine-based multitarget inhibitors showing improved target inhibitory profiles for PTR1 and DHFR of both *L. major* and *T. brucei*. Among these inhibitors, we report the first, to the best of our knowledge, apparent picomolar inhibitors of *Tb*PTR1 and several new low nanomolar inhibitors of *Lm*PTR1, which mostly also show selective micromolar to submicromolar inhibition of the parasite DHFR variants. *In vitro* evaluations of the designed multitarget inhibitors against bloodstream forms of *T. brucei brucei* revealed low micromolar to submicromolar EC_{50} values for three of these pteridines. Taken together, we here report a successful application of a systematic multitarget design approach to yield selective pteridine-based antiparasitic compounds affecting multiple trypanosomatid enzymes.

RESULTS AND DISCUSSION

Reference Compounds Inhibit both PTR1 and DHFR. To systematically assess multitarget inhibition, we measured the inhibition of *Tb*PTR1, *Tb*DHFR, *Lm*PTR1, *Lm*DHFR, and the off-targets hDHFR and hTS by the folate-related anticancer agent methotrexate (MTX, **1a**) and seven further pteridine-based reference compounds (**1b**−**1h**, Figure 2 and Table S1, SI).[26,30,32] Although **1b**−**1h** were primarily designed as *Lm*PTR1 inhibitors, we found all to be more potent against *Tb*PTR1 than *Lm*PTR1 with **1b** being the strongest inhibitor of *Tb*PTR1 with an IC_{50} of 50 nM against *Tb*PTR1 and 1 μM against *Lm*PTR1 (Figure 2A). Notably, these compounds exhibited micromolar to submicromolar inhibition of *Lm*DHFR and *Tb*DHFR (IC_{50} *Lm*DHFR 0.3−1.4 μM; *Tb*DHFR 0.3−20.05 μM). While MTX (**1a**) was more potent against the parasite DHFRs, it was not selective (selectivity index SI: *Tb*DHFR/hDHFR = 3 and *Lm*DHFR/hDHFR = 1, Figure 2A). For compounds **1b**−**1h**, higher SI values were observed, ranging up to about 165 for **1b** for both *Tb*DHFR and *Lm*DHFR (Figure 2A).

Substrate-like and Methotrexate-Inhibitor-like Binding Modes of the Reference Compounds. Despite the hydrogen-bonding network stabilizing the pteridine ring in the PTR1 active site, for the PTR1 complexes with MTX/**1a** derivatives, there are two alternative binding modes. Previously determined crystal structures show that compounds **1b** and **1c** share a substrate-like pterin orientation in the complex with *Lm*PTR1.[26] In the same crystal structure, compound **1b** also adopts a second, so-called inhibitor-like (or MTX-like) orientation, with the bicyclic ring system flipped by 180° and rotated by 30° (Figures 3A,B and S1).[26] Dual binding modes have also been observed in crystallographic complexes of *Tb*PTR1 with small pteridine-based inhibitors.[32]

We here determined the crystal structure of the ternary complex of *Tb*PTR1 with NADPH/$NADP^+$ and the reference compound **1b** (PDB-ID 6rx5, resolution 1.42 Å, experimental details: Tables S2 and S3). It shows that the diaminopteridinyl

https://doi.org/10.1021/acs.jmedchem.2c00232
J. Med. Chem. 2022, 65, 9011−9033

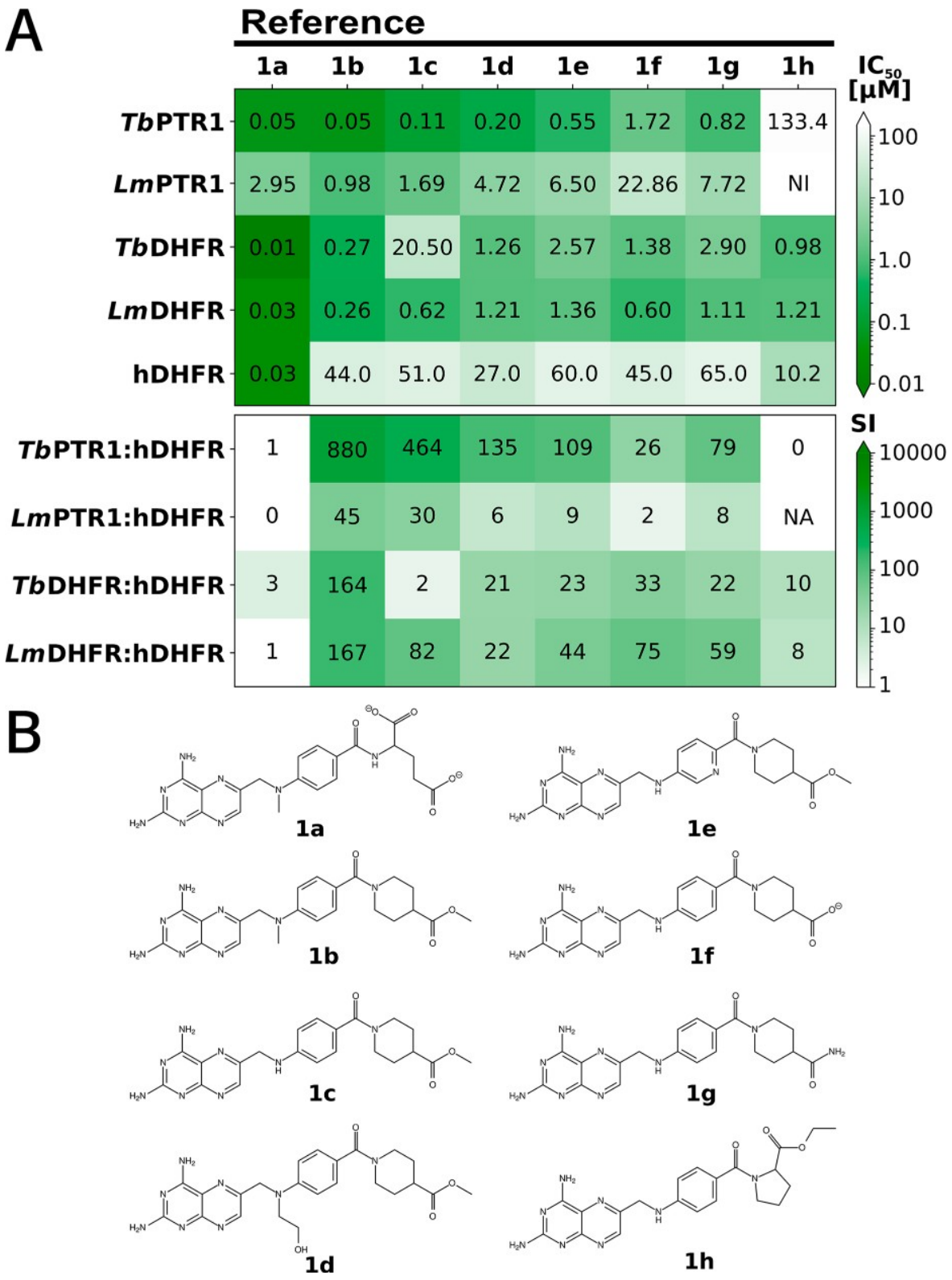

Figure 2. Inhibitory activities, selectivities, and structures of reference pteridines. (A) Heatmaps show activities given by IC_{50} values (top) and selectivity indices (SI) (bottom) for the targets and the off-target hDHFR. All values, as well as data for hTS, are given in Table S1. NI: no inhibition; NA: not applicable. (B) Previously published compounds shown were used as reference compounds: **1a** is methotrexate; **1b**, **1c**, and **1h** are **6b**, **6a**, and **6c** from Cavazzuti et al.;[26] and **1d**−**1g** correspond to **5d**, **5b**, **6a**, and **5a** from Corona et al.[30]

moiety of **1b** adopts only the MTX-like orientation (Figure 3C), resembling its MTX-like binding mode in *Lm*PTR1 (Figures 3B and S2). Consistently, docking studies indicated that all reference pteridines adopt MTX-like binding modes in the different targets and the off-target hDHFR (Table S4 and Figure S5). Therefore, we concluded that the MTX-like binding mode

https://doi.org/10.1021/acs.jmedchem.2c00232
J. Med. Chem. 2022, 65, 9011−9033

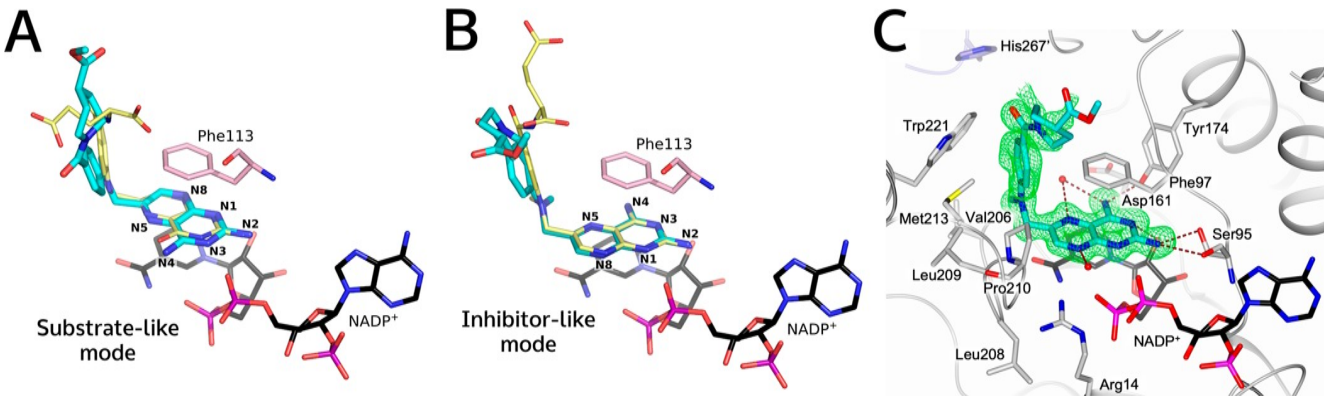

Figure 3. Orientations of reference pteridine compound **1b** in crystal structures of *Lm*PTR1 and *Tb*PTR1. (A,B) Compound **1b** (cyan carbons) in complex with *Lm*PTR1 (PDB-ID 2qhx) has a substrate-like (A) and an inhibitor-like or MTX-like (B) binding mode. **1b** is shown with (A) folate (yellow carbons) superimposed from a *Tb*PTR1 structure (PDB-ID 3bmc) and with (B) MTX (**1a**, yellow carbons) superimposed from an *Lm*PTR1 structure (PDB-ID 1e7w). The pteridine nitrogens are labeled according to the ring nomenclature. (C) Binding site in the crystal structure determined in this work (PDB-ID 6rx5) of *Tb*PTR1 (gray cartoon, His267′ from the neighboring subunit in lavender) in complex with NADPH/$NADP^+$ and compound **1b**, which has the MTX-like binding mode. Interacting residues (in A, B: only Phe113) and the NADPH/$NADP^+$ cofactor are shown in sticks (carbons colored according to protein and black, respectively). In (C), water molecules are shown as red spheres, and the inhibitor is surrounded by the omit map (green wire) contoured at the 2.5 σ level. Hydrogen bonds are represented by brown dashed lines.

is likely the dominant one, and we focused on the analysis of this binding mode in the subsequent compound design.

Comparative Target/Off-Target Mapping and Docking Studies Support Design Focused on Selective Multitarget Inhibition. To develop enhanced selective inhibitors of the parasite targets, we employed a multitarget-based design approach to improve inhibition of *Tb*PTR1, *Tb*DHFR, *Lm*PTR1, and *Lm*DHFR while retaining low hDHFR off-target inhibition. The next generation of pteridine-like compounds was created by dissecting the part of **1b** attached to the pteridine core into three modules. These were N10, the substitution to the N10 position; PABA, the *para*-amino benzoic acid (PABA) moiety; and Tail, the cyclic glutamate tail (Figure 4). We separately modified each of these modules to obtain three new series of compounds. The modifications of each module were based on binding mode predictions from docking in the different targets and the off-target hDHFR and our previously published optimization guidelines for MTX-like scaffolds.[31] The key concepts adopted in the compound design are summarized in Figure 4.

Rationale for N10 Modifications. The binding pockets of the different target proteins were found to share a number of aliphatic residues in the proximity of the N10 substituent of a bound ligand, e.g., Leu209 of *Tb*PTR1; Ile47 and Leu90 of *Tb*DHFR; Leu226 and Leu229 of *Lm*PTR1; Ile20 and Val62 of *Lm*DHFR (Figure 4A).[31] Bulkier nonpolar groups in comparison to the methyl of **1b**, like the ethyl and propargyl substituents of **2a** and **2b**, allow for interactions with those hydrophobic moieties. Docking studies suggested that even substituents of the size of benzyl, as in **2c**, can be accommodated in the PTR1 and DHFR pockets (Figure 5A,B). Furthermore, such bulky substituents may improve selectivity for the on-targets: The hDHFR pocket has a lower volume compared to the parasite DHFR pockets (pocket volume *Tb*DHFR 353 $Å^3$, *Lm*DHFR 384 $Å^3$, and hDHFR 347 $Å^3$).

Furthermore, as previously demonstrated,[31] hDHFR favors hydrogen bond donors in the proximity of N10 and the PABA ring system, whereas the parasite DHFRs allow for favorable interactions with hydrogen bond acceptors. To improve off-target selectivity, we thus replaced N10 by sulfur and the PABA benzene ring by pyridine in **2d**.

Although Corona et al.[30] found improved selectivity for PTR1 over hDHFR by hydrophilic N10 substitutions, our data for reference compound **1d** with a hydroxyethyl substituent did not support this observation (Figure 2A). Docking simulations indicated that interactions with a highly conserved structural water might induce an unfavorable conformation of the substituent's aliphatic chain (Figure S5A, SI). To relax the geometry while allowing interactions between the substituent and water, we elongated the aliphatic linkage to a hydroxypropyl in **2e**.

Thus, in total, the N10 series consists of five novel pteridines (**2a**–**e**, Figure 6) modified to improve interactions with PTR1 and parasite DHFR and to exploit the differences in pocket sizes and residues between the parasitic targets and the hDHFR off-target.

Rationale for PABA Modifications. As a first modification to the PABA moiety, in **3a**, we replaced the PABA phenyl group with benzyl (Figure 6). The additional hydrophobic spacer can interact with hydrophobic target residues while resulting in a shifted position of the hydrophilic linker amide. The positioning of hydrophobic and hydrophilic residues surrounding the PABA moiety and the amide linker in the human off-target is different from that of the parasite targets PTR1 and DHFR, which can be exploited to improve selectivity. For the same reason, the amide linker position was also shifted in **3b** by substituting the PABA moiety with *meta*-aminobenzoic acid.

A second key feature of the targets vs off-targets that was used to inform the design of the PABA series relates to the compound tail: Tail regions are solvent-exposed in PTR1 and thus have poorly defined interactions (Figure 4B). In contrast, in DHFR, the tail region is enclosed, and strong interactions occur with the hDHFR off-target.[31] We therefore shortened the tail region to achieve full enclosure in the PTR1 binding pocket by replacing PABA by naphthalene (**3c**) or benzene moieties (non-substituted, **3d**; or substituted with $-CF_3$, **3e**). Docking results showed that the smaller tail fully resides in the PTR1 binding pocket (Figure 5C) and is stabilized by surrounding hydrophobic residues, not only in PTR1 but also in parasite DHFR

https://doi.org/10.1021/acs.jmedchem.2c00232
J. Med. Chem. 2022, 65, 9011−9033

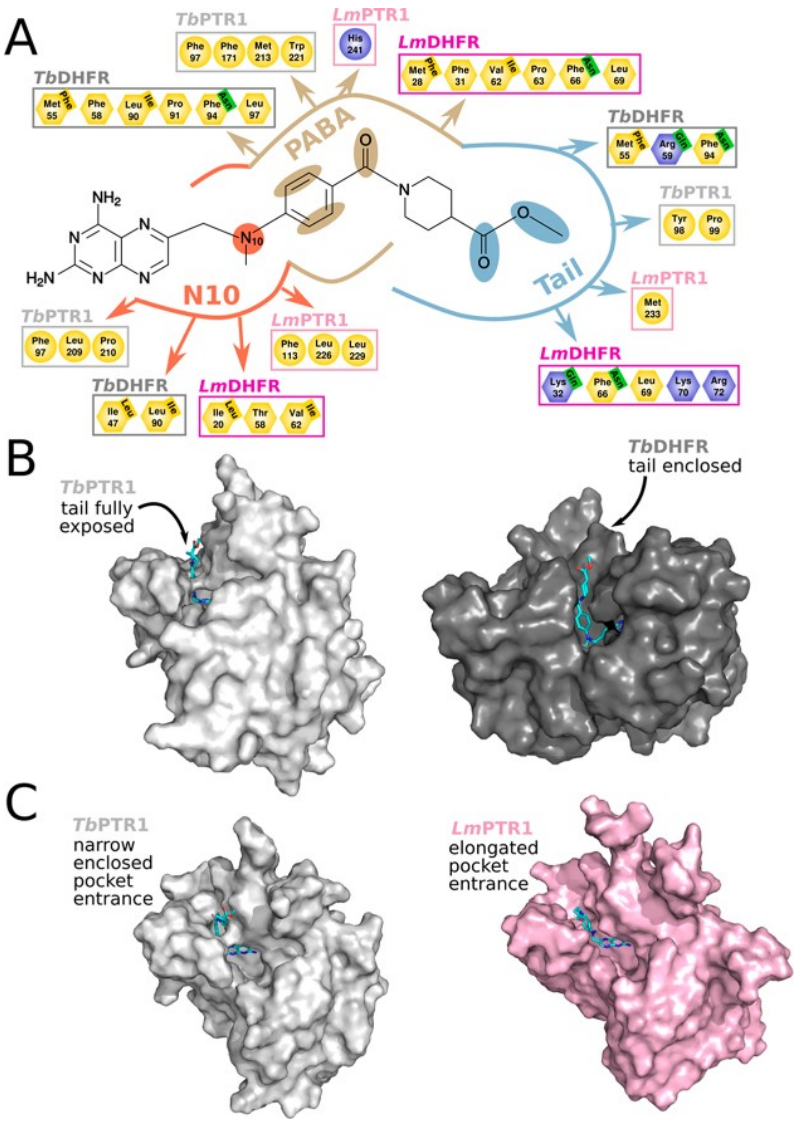

Figure 4. Structural features of PTR1 and DHFR considered in the multitarget design of selective compounds illustrated for reference compound **1b**. (A) Selected residues within 5 Å of the three modules—N10, PABA and Tail—modified in the design procedure. Residues were selected for the complexes of **1b** with *Tb*PTR1 (pale gray), *Tb*DHFR (dark gray), *Lm*PTR1 (pale pink), and *Lm*DHFR (dark pink). Residues are colored according to their properties: basic: blue, polar: green, and nonpolar: yellow. The ligand interaction plot is based on Panecka-Hofman et al.[31] and provides an overview of residues with similar properties that surround the ligand modules in the different targets (showing only those applied for the design; for full maps, see Figures S3 and S4). In some positions, the amino acid type of the off-target hDHFR is different from parasite DHFR. Differing hDHFR residues are labeled in the top right corner of the corresponding parasite DHFR residue. These positions highlight suitable substitution points to improve selectivity. (B) Surface representations of complexes of **1b** with *Tb*PTR1 (left, PDB-ID 6rx5) and *Tb*DHFR (right, MTX-like top-ranked docking pose in PDB-ID 3rg9). The compound tail moiety is fully solvent-exposed in PTR1, whereas it is well-enclosed in DHFR. (C) Surface representations of complexes of **1b** with *Tb*PTR1 (left, PDB-ID 6rx5) and *Lm*PTR1 (right, PDB-ID 2qhx, state A). The ligand is more enclosed in the narrow pocket entrance of *Tb*PTR1, while the *Lm*PTR1 pocket has an elongated, widened funnel that can accommodate larger compound tails. In (B,C), **1b** is shown in sticks with cyan carbons.

(Figure 5C,D). Rigid-body docking studies suggested that the bulky naphthalene of **3c** may be particularly beneficial in *Lm*PTR1, since this target has a more elongated, open pocket compared to *Tb*PTR1 (Figure 4C). The PABA moiety modifications are therefore suitable for modulating the compound interaction profile in a species-specific manner.

In summary, the PABA series contains five new pteridine derivatives (**3a**–**3e**, Figure 6) designed to improve selectivity by exploiting the different surroundings of bound PABA moieties in hDHFR in comparison to the parasite target proteins.

Rationale for Tail Modifications. The surrounding of the compound tail features several hydrophobic residues, particularly in the two *T. brucei* targets (Figure 4A). Directional interactions with the tail moiety may have limited benefit for the binding affinity in PTR1, since the flexibility of the solvent-exposed tail likely has an entropic contribution. Hydrophobic interactions are geometrically less restrained than, for instance, hydrogen bonds. Therefore, anticipating less pronounced entropic penalties on binding in our designed derivatives, we replaced the methyl ester in the tail of **1b** by the more flexible ethyl and propyl in **4a** and **4b**, respectively. Two aspects may

https://doi.org/10.1021/acs.jmedchem.2c00232
J. Med. Chem. 2022, 65, 9011−9033

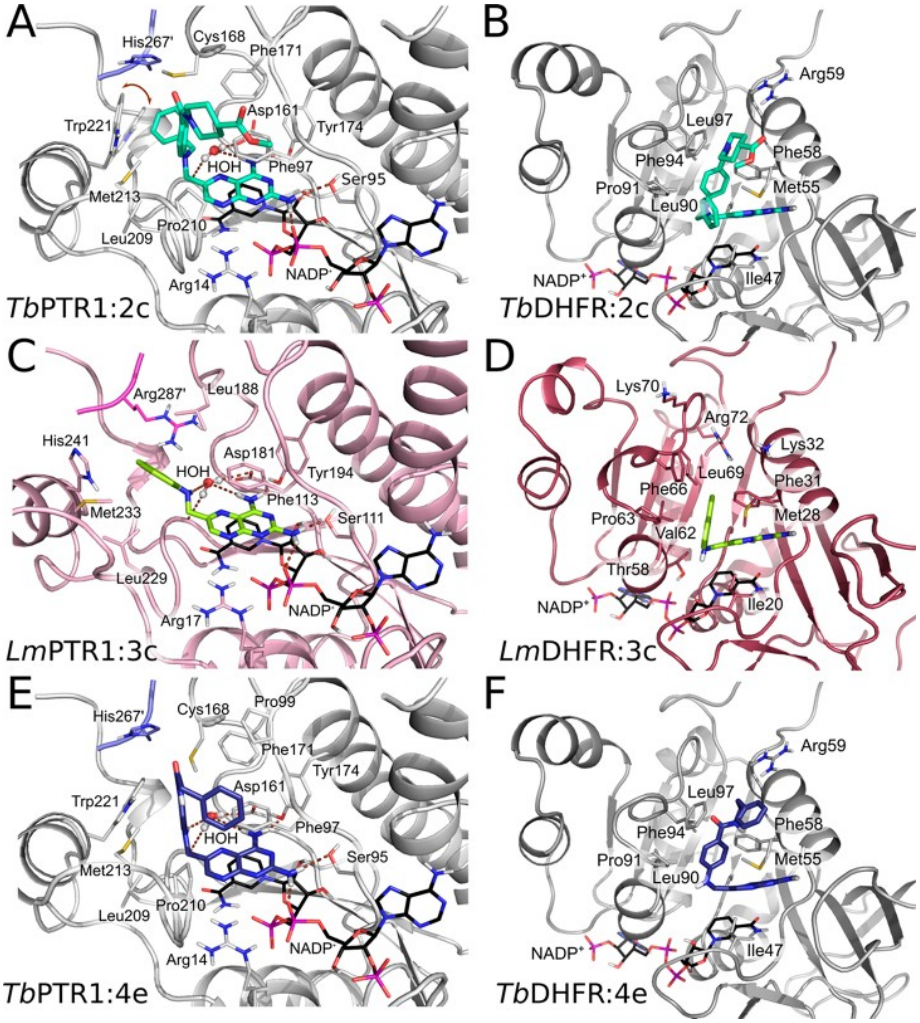

Figure 5. Views of the binding sites showing docked poses of selected pteridine-based inhibitors in the target proteins: *Tb*PTR1 (pale gray) (A,E), *Tb*DHFR (dark gray) (B,F), *Lm*PTR1 (pale pink) (C), and *Lm*DHFR (dark pink) (D). (A) Induced fit (IF) MTX-like docking pose for compound **2c** (cyan carbons) in *Tb*PTR1 in the presence of a conserved water molecule (ball-and-stick representation): Trp221 moves (indicated by a brown arrow) to make room for the phenyl of **2c**. (B–F) Rigid-body docking poses of **2c** in *Tb*DHFR (B), **3c** (lime carbons) in *Lm*PTR1 and *Lm*DHFR (C,D), and **4e** (purple carbons) in *Tb*PTR1 and *Tb*DHFR (E,F); see text for discussion. Docked poses are shown for N1-deprotonated compounds, but similar orientations were observed for the N1-protonated forms (see Figure S6). For PTR1, all docking poses shown were obtained in the presence of conserved structural water molecules. Generally, similar poses were observed for docking without water. In all panels, proteins are shown in cartoon representation with the important interacting residues (compare Figure 4A) and the NADPH/NADP$^+$ cofactor shown in sticks (carbons colored according to protein and black, respectively). Residues His267′ and Arg287′ from the neighboring subunit are shown in lavender and magenta in *Tb*PTR1 and *Lm*PTR1, respectively. Hydrogen bonds are represented by brown dashed lines. Further IF docking poses are shown in Figures S7 and S8.

result in selectivity benefits from this approach: The tail region is enclosed by more hydrophobic moieties in parasite DHFR than in the hDHFR off-target (Figure 4A), and residues surrounding the tail have previously been demonstrated to show differing conformational variability in the crystal structures when comparing parasitic targets with the off-target.[31]

To combine exploitation of the differing patterns of hydrophobic residues in the tail environments of targets and off-targets with improved enclosure in PTR1 (Figure 4A,B), we further modified the tail to an unsubstituted piperidine (**4c**) or replaced piperidine with an unsubstituted benzene (**4d**). Compound **4e**, with benzene attached via a flexible ethyl linkage to an MTX-like amide, can benefit from nonpolar and aromatic residues surrounding the tail in PTR1 and parasite DHFR and, according to docking predictions, readily adapt to their differing placements in the on-targets; see Figure 5E,F. The docking studies additionally suggest that the flexible aromatic tail can form cation–π interactions with positively charged residues in the entrance of the DHFR pocket (e.g., Arg59 of *Tb*DHFR, Figures 4A and 5F). Additional hydrophobic residues in the target pocket entrance regions, like Pro99 of *Tb*PTR1 (Figure 4A), can be targeted with an altered geometry in combination with methoxylations: **4f** and **4g** combine a one-carbon spacer between N10 and PABA and amide-linked methoxylated tail portions. In addition, an etheryl linkage to a nonsubstituted (**4h**), methoxylated (**4i**), or trimethoxylated (**4j**) benzyl group was explored. Compounds **4f–4j** were collectively designed to interact with the different hydrophobic, aromatic, and positively charged surrounding residues found around the tail region in the various targets (Figure 4A).

Taken together, the tail series comprises 10 new pteridines (**4a–4j**, Figure 6) with modified tails to target residue patterns

https://doi.org/10.1021/acs.jmedchem.2c00232
J. Med. Chem. 2022, 65, 9011–9033